IEEE Access
Multidisciplinary ⋮ Rapid Review ⋮ Open Access Journal

Received 26 July 2024, accepted 16 August 2024, date of publication 2 September 2024, date of current version 6 November 2024.

Digital Object Identifier 10.1109/ACCESS.2024.3447704

RESEARCH ARTICLE

Advanced Fuzzy Denoising Technique for Agricultural Remote Sensing: Modified Partition Filter for Suppressing Impulsive

EMADALDEN ALHATAMI, BHATTI UZAIR ASLAM, (Senior Member, IEEE), MENGXING HUANG, (Member, IEEE), AND SILING FENG

School of Information and Communication Engineering, Hainan University, Haikou 570100, China

Corresponding author: MengXing Huang (huangmx09@163.com)

This work was supported in part by the National Natural Science Foundation of China under Grant 82260362, in part by the Research on the Theory and Method of Intelligent Auxiliary Diagnosis of Prostate Cancer Based on Dual-Parameter under Grant MRI. 2023.01-2036.12, in part by Hainan Provincial Natural Science Foundation General Project under Grant 621MS019, and in part by the Research on Lesion Recognition of Lung Computed Tomography Images Based on Deep Learning and Heterozygosity of Different Networks.

ABSTRACT Image denoising is a critical challenge in digital image processing, particularly when dealing with random-value impulse noise (RVIN). Existing methods for RVIN detection and removal often struggle with poor generalization performance, requiring manual adjustment of detection thresholds or local window information. These approaches have difficulty handling severely damaged images or those with high background noise. To overcome these limitations, a novel fuzzy-based approach has been developed for RVIN detection and denoising in digital photographs. This method combines the power of K-means clustering with fuzzy logic to locate noisy pixels by identifying their closest neighbors. By effectively separating actual signal points from misleading noise signals during the detection phase, the proposed technique ensures precise identification of RVIN. Furthermore, a robust partition decision filter is employed in the elimination phase, effectively removing the identified noise while preserving the underlying signal. The integration of fuzzy techniques enhances the robustness and adaptability of this method, allowing it to handle various noise types and challenging image conditions. Extensive simulations using diverse remote-sensing datasets corrupted with RVIN demonstrated the superior performance of the proposed fuzzy denoising technique. It achieved an impressive 90% success rate in noise detection and maintained high accuracy even at increased noise levels, outperforming other commonly reported methods. This innovative fuzzy-based approach offers a promising solution to the problem of RVIN detection and denoising in digital images. By leveraging the advantages of fuzzy logic and K-means clustering, it provides improved generalization, increased adaptability, and enhanced noise removal capabilities, making it a significant advancement in the field of image processing.

INDEX TERMS Fuzzy denoising technique, image denoising, pixel clustering, sub region filtering, medical images, remote sensing images.

I. INTRODUCTION

In the process of acquiring, transmitting, and processing images, noise is inevitably introduced, leading to a significant decrease in image quality [1]. Two common types of noise are Gaussian and impulsive, with impulsive noise further categorized into salt and pepper noise (SPN) and random-value impulse noise (RVIN) [2]. While various noise removal algorithms exist, their effectiveness for random impulse noise is often limited. Linear and nonlinear methods, filters such as the Gaussian, mean, and bilateral filters, have been attempted for RVIN removal but struggle to preserve fine details. The median filter, as well as its variant known as the Weighted Median (CWM) filter, have demonstrated efficacy in mitigating the presence of impulse noise. However, these filtering techniques may

The associate editor coordinating the review of this manuscript and approving it for publication was Qichun Zhang.

inadvertently misclassify and remove pixels that are actually clean, particularly in image regions characterized by detailed textures [3], [4].

To overcome these challenges, a denoising algorithm consisting of two stages, which based the detection and filtering of noise, has been put forward. The accuracy of noise detection plays a crucial role in achieving optimal denoising results [5]. A variety of noise detection methodologies have been introduced in the literature, including the Local Rank-Ordered Absolute Difference (ROAD), Rank-Ordered Logarithmic Difference (ROLD), and Rank-Ordered Relative Differences (RORD) techniques [6]. Additionally, noise detection thresholds can be influenced by the noise level, and methods like the local consumer's index (LCI) have been used to estimate the noise level and set appropriate thresholds.

Single-threshold detection methods may lead to misjudgments for images with complex textures and severe damage. Multi-threshold methods based on standard deviation, average value, and quartile have been developed, but they increase complexity without significantly improving noise detection [7]. Fuzzy noise detectors utilizing switching technology have been suggested to differentiate noise pixels from edge pixels within detailed and textural regions [8].

However, Current techniques frequently depend on local pixel data within a confined window range and overlook the comprehensive pixel distribution features of the entire image [9]. Points and lines form the underlying framework that shapes and supports the design of spires. While median filters and their enhanced algorithms can effectively remove noise from images, for detailed textures containing elements like points, lines, and spires [10]. These techniques may inadvertently remove clean pixels within the fine details and textures, incorrectly identifying them as noise [11]. This can result in the persistence of image blur and the loss of important detailed information. The proposed a methodology for detecting and eliminating RVIN through the utilization of grouping clustering techniques, aimed at mitigating associated challenges effectively. The noise detection algorithm categorizes pixels into clusters according to their unique attributes, refining the noise detection process through iterative optimization. This iterative approach establishes the most effective detection thresholds tailored to the characteristics of each pixel cluster. Leveraging the insights derived from the noise detection analysis, a partition-based decision filter has been designed to facilitate the recovery of pixels that have been corrupted by RVIN. This approach selectively applies different filtering techniques to the noise-affected pixels versus the remaining image regions, with the goal of effectively restoring the damaged content. Extensive experimental results demonstrate the effectiveness of the proposed approach pertains to the management of noise in both original image and medical image characterized by medium level to high level of noise. It surpasses other sophisticated RVIN filtering methods significantly in both visual and objective quality assessment.

The contribution is summarized as follows:

(a) A novel approach to pixel clustering is introduced, leveraging both comprehensive and partial data extracted from the impaired image. This method aims to categorize all pixels within the damaged image into distinct classes.

(b) The optimal noise detection threshold is determined for each distinct pixel grouping through the optimization of the noise detection model. Subsequently, the LCI methodology is employed to compute the local consistency index value for those pixels belonging to the same class, with the objective of selectively filtering out the noise-corrupted content.

(c) A conceptual framework for partitioning decision-making is introduced, aimed at enhancing image quality through noise reduction. Specifically, two filtering techniques, to overcome the challenge of noise suppression within varying image regions, two distinct filtering techniques have been devised. The LCI-weighted mean filter is tailored to handle uniformity-dominated areas, while the edge direction filter is specifically designed to manage regions characterized by intricate details and sharp edges.

II. RELATED WORKS

In this section, we discuss these two stages and types of noise, the two-stage approach of impulsive noise detection and image restoration can provide an effective solution for impulsive noise reduction in digital images.

In the first stage, impulsive noise detection, the aim is to identify the pixels that are affected by the impulsive noise. Various approaches can be used for impulsive noise detection, including threshold-based methods, morphological operations, and machine learning-based techniques. Once the impulsive noise is detected, the noisy pixels can be marked or flagged for further processing.

In the second stage, image restoration, the aim is to restore the noisy pixels that were identified in the first stage. Various image restoration techniques can be used, such as median filtering, mean filtering, adaptive filtering, and deep learning-based methods. The choice of restoration technique depends on the severity of the noise and the specific requirements of the application, such as the preservation of image details and the computational complexity.

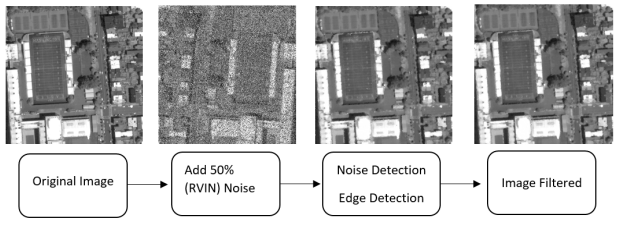

FIGURE 1. Denoising impulse noise RVIN filtering technique.

A. TYPES OF NOISE MODELS

The conceptual framework for denoising image models is depicted as $Y = X + B$, where Y represents the corrupted

image, X denotes the pristine image, and B signifies the adaptable noise component. Diverse forms of noise, such as Gaussian, Poisson, multiplicative, and RVIN, are commonly encountered in natural and medical image datasets. These noise types induce distinct alterations, as illustrated in Figure 2. Within this visual representation, f(x, y) and g(x, y) respectively denote the noisy and pristine images, while h(x, y), η(x, y), m(x, y), and p($*$) represent the probability distribution functions associated with the different noise modalities [12], [13].

Several algorithms have been developed for effective removal of Gaussian noise, and they generally perform well. However, RVIN poses unique challenges compared to other types of noise. RVIN is characterized by independent gray values randomly taken within the range of [0, 255]. RVIN noise pixels' exhibit luminance values that fall within the acceptable range for image pixels. The difference between these pixel values and the luminance values of the surrounding pixels is typically quite small, rendering the identification of RVIN noise challenging. Consequently, the elimination of RVIN noise presents greater difficulty compared to other noise types [14].

RVIN is a composite noise model that incorporates the characteristics of two distinct noise types: random-valued noise and impulse noise. Random-valued noise refers to noise where the pixel values are randomly altered, while impulse noise involves replacing some pixels with either the minimum or maximum possible value. The presence of impulse noise within RVIN can lead to significant distortions in the image, making it more difficult to remove the noise without causing further damage. Moreover, RVIN can occur in any color channel or multiple channels simultaneously, further complicating the noise removal process.

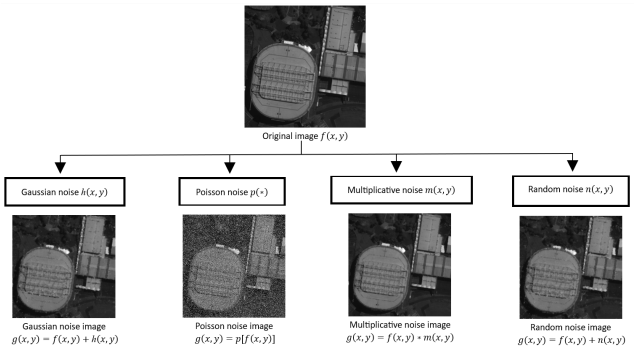

FIGURE 2. The flowchart of types of noise.

B. DETECTION OF NOISE

The approach that leverages local information statistics often involves defining a specific statistical metric or parameter, calculating RVIN is identified through a direct comparison of statistical measures obtained for individual pixels against a predetermined threshold, as discussed in the literature [15], [16]. An exemplar of this detection approach is elucidated by Singh [16] through the development of the ROAD method. In ROAD, the disparity is computed and sequentially arranged in increasing order between the focal pixel and its neighboring pixels within a defined vicinity. Subsequently, the central pixel is categorized as either pristine or contaminated based on a pre-established threshold for ROAD detection. It is noted that the ROAD algorithm demonstrates proficient performance particularly in scenarios characterized by low levels of image noise [17], [18].

Through the utilization of the logarithmic function on the absolute variances, [19] introduces a novel metric termed ROLD, designed to enhance the discrimination between noisy and clear pixels. Even amidst noise densities reaching 60%, ROLD's detection capability surpasses that of ROAD, primarily due to its enhanced ability in discerning between noisy and non-noisy pixels. Subsequently, researchers have formulated several advanced algorithms, including ROR and ROD-ROAD, building upon the foundational concepts of ROAD and ROLD [20]. However, impulsive noise reduction remains an ongoing challenge, and further advancements in methods are still needed.

A novel method for detecting noise has been developed, utilizing the local statistical measure termed the local Consensus Index, drawing insights from the ROAD algorithm and the bilateral filter. This approach evaluates the similarity of a pixel x to its neighboring pixels to determine its noise characteristics [21], [22]. The specific computational methodology is elucidated in Formulas (1) and (4):

$$\theta(x,y) = \exp\left(-\frac{||\overrightarrow{(s,t)} - \overrightarrow{(m,n)}||^2}{2\sigma_\lambda^2}\right) \cdot \exp\left(-\frac{||u_x - u_y||}{2\sigma_s^2}\right), y \in \Omega_x^o \tag{1}$$

In Equation (1), θ *(x, y)* denotes the measure of likeness between the pixel values at local coordinates x and y. Here, y denotes any pixel within the vicinity, while Ω_x^0 denotes the matrix 5 $\times$ 5-pixels neighborhood surrounding central pixel x, excluding x itself. The grayscale intensity levels associated with the x and y of the pixels are denoted as Ω_x^0, u_x, and u_y, respectively, with their corresponding coordinates represented by *(m, n)* and *(s, t)*.

$$\xi x = \sum_{y \in \Omega_x^o} \theta(x,y) \tag{2}$$

The Gaussian kernels, denoted as σ_λ and σ_s are utilized to adjust the influence of both pixel intensity variation and spatial separation on the parameter θ *(x, y)*. From Formula (2), it is evident that in the case where x represents a regular pixel, the magnitude of ζx is expected to increase as a result of its close resemblance to all other typical pixels within its vicinity, and conversely.

$$\overline{\xi x} = \xi x / \overline{\sum_{\mathrm{y} \in \Omega^{\mathrm{o}}} \xi y} \tag{3}$$

Through the examination of the x-coordinate value associated with the central pixel, x.

$$LCI_x = \begin{cases} 1, & \overline{\xi x} > 2.5 \\ \overline{\xi x}/2.5, & \overline{\xi x} \leq 2.5 \end{cases} \quad (4)$$

Hence, through examination of the ξx value associated with the central pixel x as described in Formula (3), an evaluation can be made regarding the probability of its classification as a typical pixel. Utilization of Formulas (3) and (4) by the researcher serves to confine the statistic ξx within the range [0, 1], thereby enhancing its capacity for differentiation and reliability. Consequently, this methodology facilitates the determination of the LCI (Likelihood of Classification as Intact) value for pixel x.

The LCI provides a measure of the likelihood that a pixel is noise, where higher LCI values indicate a higher probability of the pixel being a normal pixel [23]. By choosing an appropriate threshold value, it is possible to efficiently eliminate both clear and distorted pixels throughout the entirety of the compromised image. To enhance the efficacy of detection outcomes, the author employs LCI initially to differentiate between regions with uniform texture and those with intricate details. Subsequently, various LCI thresholds are applied to filter out extraneous noise. This approach, characterized by computational simplicity, facilitates prompt identification of Retinal Vascular Injuries RVIN within impaired image datasets, obviating the necessity for iterative procedures [24].

III. PROPOSED METHOD (FUZZY C MEAN BASED NOISE DETECTION AND CLUSTERING OF IMAGE PIXELS METHOD)

The proposes a method for detecting and clustering noisy pixels in images using the Fuzzy C Mean (FCM) algorithm. The FCM algorithm is a popular clustering technique that assigns membership values to each pixel, indicating its degree of belongingness to different clusters. The proposed method first applies a noise detection technique to identify noisy pixels in the image. This technique utilizes statistical measures such as mean and standard deviation to differentiate between noisy and noise-free pixels. The FCM algorithm is then employed to cluster the remaining noise-free pixels into distinct groups based on their similarity.

The utilization of LCI detection thresholds tailored to the structural attributes and edge complexity of images represents an effective strategy for enhancing the identification of noisy pixels. These pixels, typified by erratic value dispersion and random spatial distribution across the image, pose challenges to conventional noise detection algorithms primarily centered on value-based characteristics. However, emerging research has proposed a novel methodology that incorporates a stochastic process model to analyze point patterns generated by random noise [25], thereby capturing the spatial randomness. This method involves clustering image pixels based on their relative positions and intensities to distinguish between damaged and undamaged pixels. Despite its innovative framework, proposed pixel classification technique, which is predicated upon a stochastic process model, has been meticulously designed, yet its performance tends to yield only moderately satisfactory outcomes.

A substantial body of literature [26] underscores the observation that pixels within regions bordered by edge contours exhibit coherence and resemblance, manifesting as minimal distances among pixels belonging to the same region. Acknowledging this phenomenon, the authors propose the adoption of edge-aware geodesic distance as contour cues to formulate a structured edge detector, which addresses common challenges encountered during optical flow computation, such as occlusion and motion boundaries. Furthermore, geodesic distance serves as a valuable asset in conducting edge-preserving manipulations in image editing tasks, such as texture flattening and denoising [27]. Drawing inspiration from the findings of [6] and [15], the comparability of geodesic distances among pixels is utilized to classify all pixels within the corrupted image. Consequently, solely pixels belonging to the same classification in proximity to the central pixel are considered in the determination of the LCI value of the edge, thereby incorporating prior knowledge. Finally, to enhance robustness, distinct LCI detection thresholds are established based on the characteristics of each individual pixel category.

Various data clustering methods, including expectation-maximization (EM) clustering, Gaussian Mixture Model (GMM), density-based clustering (DBSCAN), and mean shift clustering, are available for analysis. The K-means algorithm was selected as the segmentation approach due to its inherent simplicity and propensity for rapid convergence. K-means image clustering segmentation, also commonly referred to as K-means clustering, is an unsupervised learning technique employed to categorize pixels into multiple distinct clusters. The subsequent principles outline its specific application:

- In the context space of d-dimensional Euclidean and a known number of clusters K, clustering analysis is employed to group data points $(x_1, x_2, \ldots, x_n)$ based on their proximity in Euclidean distance [28].
- The involves identifying K clustering centers, denoted as $\mu_k(k= 1, 2, \ldots, k)$, and assigning each pixel in a damaged image to its nearest clustering center. The objective is to minimize the sum of squared differences between each pixel's grayscale value and the corresponding clustering center. To facilitate this assignment, a binary variable $r_{nk}$is introduced, where K represents the total number of clusters and N represents the total number of pixels. Formally, if a pixel belongs to the K cluster, then $r_{nk} = 1$; otherwise, it is 0. Consequently, a loss function is defined as follows:

$$J = \sum_{n=1}^{N} \sum_{k=1}^{K} r_{nk} ||x_n - \mu_k||^2 \quad (5)$$

- Formula (5) demonstrates the necessity of initializing the value of μ_k randomly to derive the attribution value

r_{nk} for a pixel that minimizes the loss function J. With the grayscale value of pixel x_n and cluster center μ_k, given, the loss function J manifests as a linear function of r_{nk}. Since x_n and x_{n-1} are statistically independent, each pixel x_n merely requires assignment to its closest cluster center, expressed as:

$$r_{nk} = \begin{cases} 1 & \text{if } k = \arg\min_j ||x_n - \mu_j||^2 \\ 0 & \text{otherwise} \end{cases} \tag{6}$$

- By utilizing the r_{nk} obtained in Formula (6) and substituting it into Formula (5), then cluster center μ_k can be determined. With r_{nk} value given; the loss function J assumes a quadratic form with respect to μ_k. Setting the derivative of J with respect to μ_k to zero then:

$$\sum_{n=1}^{N} r_{nk}(x_n - \mu_k) = 0 \tag{7}$$

It can be inferred that the numerical representation of μ_k is

$$\mu_k = \frac{\sum_n r_{nk} x_n}{\sum_n r_{nk}} . \mu_k$$

The variable μ_k denotes the average grayscale value computed from the pixels associated with the specified class.

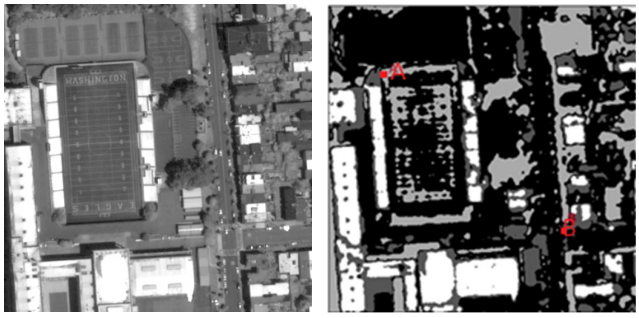

(a)

28	70	77	24	26
33	98	121	80	23
124	68	73	71	35
204	190	67	46	91
189	114	15	111	55

(b)

35	63	95	32	45
46	92	111	75	34
114	71	78	102	40
199	121	59	51	89
153	98	66	100	45

(c)

FIGURE 3. (a) playground original image, (b)noise level 50% when K=4 of clustering playground image, classification pixel of pints A and B.

To enable the efficient implementation of this process, the algorithm computes the 1D spatial separation between the pixels neighboring the central cluster pixels. Subsequently, a distinct category is delineated by aggregating the pixels proximal to the central cluster. By specifying a value for K, the image pixels can be effectively organized into K clusters. This approach to pixel clustering serves to partition complex textural elements within images, thereby enabling systematic processing within each category and bolstering the efficacy of image restoration efforts.

Figure 3(b) illustrates the clustering effect on the Barbara image with 50% RVIN when K equals 4. In Figure 3(c), the image pixels are partitioned into three distinct categories, each visually represented using a unique color. Leveraging the outcomes of this pixel clustering process, the pixels belonging to the same category can be subsequently utilized to compute the LCI value associated with the central pixel under consideration. For example, in Figure 3(c), the central pixel of region A only has 8 neighboring pixels (77, 24, 26, 121, 80, 23, 71, 35) from the same category out of the 24 neighboring pixels. Therefore, when computing the LCI value for the central pixel x, the algorithm selectively considers only the pixels belonging to the same category, thereby leveraging this prior knowledge regarding the presence of edges to enhance the accuracy of the LCI estimation. It should be noted that the K-means algorithm has poor interference tolerance, so the method preprocesses the images by applying simple filtering techniques like median filtering or Gaussian filtering before clustering and segmenting the images. This preprocessing step reduces the impact of noise on the clustering results, meeting the requirements for subsequent experiments.

In the filtering stage, different filters are applied based on the noise pixels' locations in other regions. Rather than relying on existing or enhanced median filters, the proposed method employs a more robust partition-based decision filter to effectively mitigate and remove the detrimental impacts of RVIN. The proposed partition decision filter takes into account both image features and noise regions simultaneously. It selectively filters the central pixel by considering only the neighboring pixels that have been determined to be reliable.

A. LCI FILTER

The LCI weighted mean filter is intended to correct the noisy pixels that are determined in a flat area. Formula (8)'s LCI weighting filter:

$$I'_x = \frac{\sum_{y \in \Omega_x^o} [LCI_y^2 \cdot I_y]}{\sum_{y \in \Omega_x^o} [LCI_y^2]} \tag{8}$$

Let I_x represent the grayscale value of the noise-contaminated pixel x after filtering, and I_y denote the grayscale value of the pixel y, which was classified as a clean, uncontaminated pixel during the preceding noise detection stage and resides within the local neighborhood Ω_x^0. Additionally, let LCI_y represent the LCI value associated with pixel y.

The LCI value of each neighboring pixel is employed as the weighting factor within the filtering operation, as the LCI serves as a proxy for the probability that the given pixel is indeed clean and unaffected by noise. The rationale is that pixels with larger LCI values, indicating a higher likelihood

of being noise-free, should be granted greater influence in the reconstruction of the central noise-corrupted pixel.

Assuming that the grayscale distributions of pixels situated in relatively flat, homogeneous image regions tend to exhibit smooth variations, the employment of a filter window that is overly large risks the inclusion of pixels located along edges and in textured areas. thus, the filter window size for the proposed LCI-weighted filtering approach is judiciously set to matrix 5×5 pixels.

B. DIRECTION FILTER OF EDGE

To overcome the presence of noise pixels within edge and detail-rich areas, a specialized filter termed the 'edge direction filter' has been designed. This filter leverages the observation that the gray level values of pixels located within the neighborhood undergo pronounced, sharp changes. However, due to the inherent characteristics of edges, there invariably exist pixels in a particular directional orientation wherein the gray level difference is negligible. The edge direction filter operates by adhering to the following methodological steps:

(1) If the event that a given pixel, denoted as x, is identified as a noise-induced pixel situated within an edge or detail-rich region, an M×M detection frame is subsequently constructed, with the pixel x positioned at the center of this frame.

(2) Based on the noise classification results from the first stage, clean pixels are selected from the four lines of the detection frame. The pixels that have been designated as clean, noise-free pixels, situated along the row, column, left diagonal, and right diagonal axes relative to the current central pixel, denoted as x, are respectively categorized and stored within the distinct sets D_h, D_v, D_l, and D_r, as depicted in Figure 4(b).

(3) The standard deviation of the elements contained within each of the aforementioned sets, D_h, D_v, D_l, and D_r, is subsequently calculated. The directional axis represented by the set exhibiting the lowest standard deviation is then selected and designated as the boundary filtering direction, denoted as D_f.

(4) The grayscale intensity values associated with the clean, noise-free pixels situated along the designated boundary filtering direction, D_f, are then sorted in ascending order. Subsequently, the median value within this sorted sequence is selected and assigned as the updated grayscale intensity for the central pixel, denoted as x, which had initially been identified as a noise-induced pixel.

To demonstrate the operation of the edge direction filter, a specific edge region from Figure 4(a) has been selected, and the corresponding pixel grayscale distribution is presented in Figure 4(c). The elements in the four-direction sets of this region are $D_h = [105, 98, 85, 216]$, $D_v = [178, 212, 95, 17, 58]$, $D_l = [89, 85, 181]$, and $D_r = [146, 118, 72, 48]$. By computing the standard deviation for each set of values, it is observed that the D_v direction corresponds to the edge direction. Additionally, visually inspecting Figure 4(c) confirms that the calculated edge direction aligns with the visually apparent edge direction. Subsequent to the application of the median filtering operation, the grayscale intensity value associated with the central pixel is determined to be 99 within the set D_v, which closely approximates the ground truth intensity value of 93 for this particular pixel.

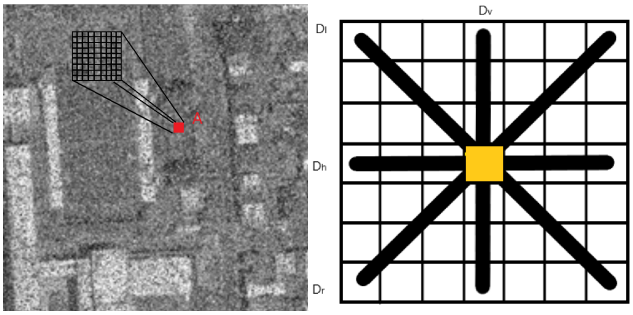

89	112	67	58	97	41	48
61	205	81	17	183	56	126
22	99	216	95	72	68	183
105	107	98	213	85	83	216
120	201	118	212	85	83	87
124	209	18	244	139	25	28
146	87	113	178	164	176	181

(c)

FIGURE 4. (a) 50% RVIN playground Image, marked as the edge point A, (b) the sets of Dh, Dv, Dl and Dr, (c) the noise of pixels in red color.

To ensure effective filtering, the improved median filter utilizes a window size of 7×7. If the filter window is too small, there is a risk of having a limited number of clean pixels in the edge direction. This can lead to the presence of artifacts and blurring in the image, ultimately compromising the quality of the filtering outcome.

IV. EXPERIMENTS AND DISCUSSIONS

To rigorously evaluate the efficacy of the proposed denoising approach, a series of noise detection and removal experiments were conducted across a diverse set of remote sensing imagery. The test image dataset, as illustrated in Figure 5, comprises the following scenes: (a) storage tanks, (b) beach, (c) runway, (d) buildings, (e) road intersection, (f) airplane, and (g-i) three variations of a playground. All images within the test set have dimensions of 512×512 pixels.

To comprehensively assess the performance and efficacy of the proposed two-stage denoising algorithm, both quantitative and qualitative evaluation methodologies were employed. The assessment metrics utilized in this study encompass widely adopted indices such as the Miss Detected (MD) pixel count and False Detected (FD) pixel count, which serve to directly evaluate the noise detection capabilities. Additionally, the Structural Similarity (SSIM) index and

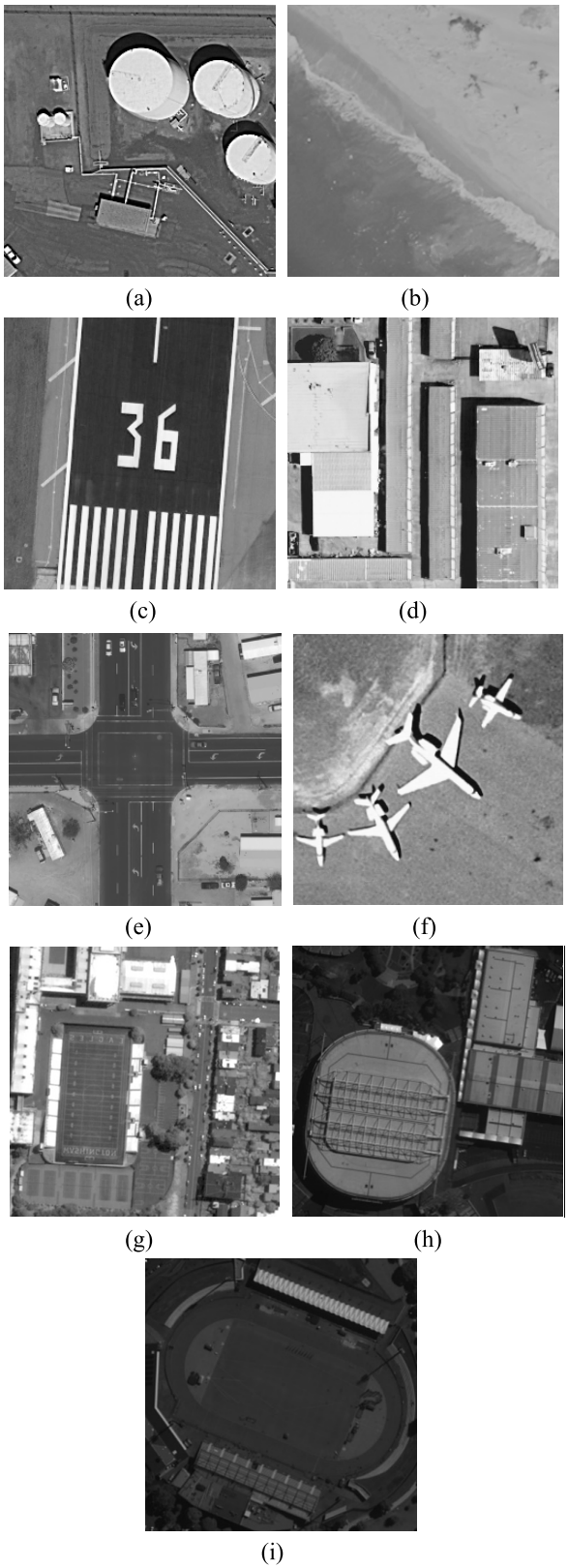

FIGURE 5. Test of denoise images: (a) Storage tanks, (b) Beach, (c) Runway, (d) Buildings, (e) Intersection, (f) Airplane, (g) Playground, (h) Playground-2, (i) Playground-3.

Peak Signal-to-Noise Ratio (PSNR) metric were employed to assess the overall quality of the filtered imagery.

Through the application of these diverse evaluation measures, a thorough characterization of the proposed denoising technique's effectiveness can be obtained, considering both the accuracy of the noise detection stage as well as the quality of the final denoised output.

A. PROPOSED NOISE DETECTOR

The performance characteristics of the noise detection mechanism significantly influence the overall noise removal capabilities of the filtering approach. An effective noise detector should exhibit a low rate of missed detections (MD), a low rate of false detections (FD), and a high accuracy in correctly identifying actual noise pixels (True Hit rate).

The detection results of the proposed noise detection technique, assessed across test imagery exhibiting varying noise levels, are presented in tabular form in Table 1. This data illustrates that images with relatively simpler grayscale pixel value distributions and less intricate textural content, such as those depicting storage tanks, beaches, runways, buildings, intersections, and airplanes, generally exhibit better noise detection effects, characterized by notably lower MD and FD pixel counts. This can be attributed to the fact that noise pixels occurring in relatively flat image regions are generally easier to reliably identify compared to those situated along edges and in textured areas.

While images containing more complex details and textures may demonstrate relatively poorer detection performance at lower noise levels, as the noise density increases, the proposed detector's ability to accurately identify noise pixels in these more challenging scenes gradually improves. This can be explained by the observation that higher noise levels result in fewer clean, uncontaminated pixels within the image, leading to more pronounced differences in grayscale intensity distributions among pixels within the detection window. Consequently, if the central pixel is noisy, it becomes easier to correctly classify it as such due to the greater dissimilarity exhibited relative to the surrounding neighborhood.

It is important to note that when the noise level is increased to reach 80% of the maximum possible value, the True Hit rate metric, which represents the proportion of correctly identified edge pixels, exceeds 90% for the vast majority of the test images evaluated across the conducted experiments, indicative of the robustness and stability of the proposed noise detection methodology.

TABLE 1. Detection for various images when RVIN 30%˜80%.

Noise density	30%		40%		50%		60%		70%		80%	
Image	FD	MD	FD	MD	FD	MD	FD	MD	FD	MD	FD	MD
Storage tanks	3899	7484	4868	10368	6717	11432	7781	13467	11985	13646	15263	15934
Beach	3199	9346	3676	11287	6130	12745	8348	13805	10596	1436	16012	17471
Runway	788	2305	1161	2884	1655	3117	2106	3128	2580	3609	3545	4180
Buildings	4719	13556	7301	16002	9566	18030	13005	18369	16741	17878	19983	19179
Intersection	2180	8297	3957	9874	4884	11885	6556	13263	10942	13215	16933	15680
Airplane	2146	5768	3385	6776	4839	7421	6536	8078	8808	9356	14803	13395

When the absolute magnitude of the difference between a given pixel's value and the value of its immediately neighboring pixel is less than 8 units, it becomes challenging

for human eyes or noise detectors to discern grayscale images. In such cases, the absolute difference between the grayscale intensity value of noisy pixels and their original true intensity value is less than or equal to 8 units, and the presence of such pixels does not result in a significant degradation of overall image quality. Consequently, these noise pixels can be considered as clean pixels. By examining the gray values of the missed noise pixels in the test images, it is observed that the majority of these pixels, in images with 30% to 80% Relative Variance of Image Noise (RVIN), have gray values within 8 bits of their true values. This further confirms the high accuracy of the proposed noise detector in noise detection.

To conduct an objective assessment of the effectiveness of the proposed noise detection methodology, a comprehensive comparative analysis was carried out by evaluating its performance against a variety of recently introduced as well as established noise filtering algorithms, including Adaptive Center Weighted Median (ACWM), Non-Local Means (ROR-NLM), Directional Weighted Median (DWM), Luo's method, Adaptive Switching Median (ASWM), Standard Deviation Obtaining Optimal Direction (SDOOD), Switching Bilateral Filter (SBF), and Contrast Enhancement-Based Filter (CEF).

As detailed in the tabulated results presented in Table 2, while certain methods, for instance Luo's approach, exhibit a low number of falsely detected pixels, they also suffer from a high rate of missed detections, which can introduce more prominent artifacts in the filtered imagery and adversely impact the performance of subsequent processing stages. In contrast, the proposed noise detection technique, although exhibiting a relatively higher number of false positive identifications, maintains an optimal overall count of correctly classified noisy pixels across different noise levels. Notably, as the noise density increases, the missed detection rate of the proposed detector progressively approaches the optimal outcome, indicating its robustness in accurately identifying noise pixels even under higher noise conditions.

Fundamentally, an effective noise detection mechanism should demonstrate the capability to identify the majority of noisy pixels while minimizing erroneous judgments. Considering the various quantitative evaluation metrics, the proposed noise detection methodology is shown to outperform the alternative approaches, exhibiting significant improvements in overall detection performance.

B. RESTORATION PERFORMANCE FILTER ON REMOTE SENSING IMAGES

To assess the effectiveness of proposed filter a comparison was conducted with several widely used filters, including ACWM, ROR-NLM, DWM, Luo's method, ASWM, SDOOD, SBF, CEF, AEPWM, and the results from these studies were considered for validation purposes. The performance evaluation was conducted using the PSNR indicator, which measures the similarity and dissimilarity between the original image and the reconstructed image, and the SSIM indicator, which characterizes the filter's ability to preserve details and characteristics.

TABLE 2. Storage tanks and Beach images contaminated by RVIN with different noise levels 30%∼60%.

Noise density	Storage tanks 30%		Storage tanks 40%		Storage tanks 50%		Storage tanks 60%	
Method	FD	MD	FD	MD	FD	MD	FD	MD
ACWM [6]	1604	12283	1928	14249	3602	20596	6668	31165
DWM [12]	4497	8530	7937	11600	8652	15035	14215	15373
ROR-NLM [22]	2841	9064	3056	12443	3655	15778	5917	21601
Luo's [28]	1225	12932	1713	14365	2135	20236	2886	33374
ASWM [29]	4321	9727	14048	7381	11042	18423	12050	10614
SDOOD [30]	6754	8598	10326	13299	15588	11741	18243	16993
SBF [31]	1225	12484	13709	2063	21063	23126	3195	24903
CEF [32]	4597	8720	13317	8037	10860	18897	8722	14935
Proposed	**3980**	**9371**	**4408**	**10368**	**6717**	**11432**	**7781**	**13467**
Noise density	**Beach 30%**		**Beach 40%**		**Beach 50%**		**Beach 60%**	
Method	**FD**	**MD**	**FD**	**MD**	**FD**	**MD**	**FD**	**MD**
ACWM [6]	7857	12720	10882	17848	13963	21171	16577	26696
DWM [12]	10955	13333	12732	15729	14747	17224	18435	20415
ROR-NLM [22]	9727	11385	13181	15817	17116	18653	20335	20772
Luo's [28]	10527	14762	12669	16804	17272	21196	18371	27599
ASWM [29]	12964	15063	13462	17751	18453	22358	21478	28856
SDOOD [30]	8238	14214	12018	17133	15367	18255	17099	18908
SBF [31]	10889	14584	13643	17083	15128	20007	17642	20383
CEF [32]	7783	10655	9248	13859	13094	16394	15741	18207
Proposed	**3199**	**9346**	**3676**	**11287**	**6130**	**12745**	**8348**	**13805**

The PSNR and SSIM values reported as the optimal results for alternative filter methodologies in their respective prior studies were selected as the comparative references. The comparative analysis findings for PSNR are presented in tabular form in Table 3 and visualized graphically in Figure 6, while the SSIM-based comparative results are detailed in Table 4 and Figure 7, demonstrate that the proposed filter exhibits superior performance on images, particularly at a noise level of 50% to 60%. Additionally, as the noise level increases, The PSNR metric for the filter method proposed demonstrated a more gradual rate of decay in value when compared to alternative filter approaches. This can be attributed to the fact that the designed noise detector in the proposed filter is capable of detecting more noise at higher levels of noise.

TABLE 3. PSNR value for different images corrupted when RVIN 40%˜60%.

Method	playground			Runway			Airplane2			Intersection		
	40%	50%	60%	40%	50%	60%	40%	50%	60%	40%	50%	60%
ACWM [6]	29.58	24.63	21.4	29.89	25.4	21.53	23.52	21.41	19.12	26.74	24.5	21.45
DWM [12]	30.86	28.51	26.35	29.13	27.25	25.42	23.95	22.71	21.22	26.67	25.30	23.42
ROR-NLM [22]	30.45	28.88	26.59	29.68	27.89	25.45	24.31	22.88	21.31	27.32	25.39	24.19
Luo's [28]	30.55	28.09	24.79	29.43	26.85	23.75	23.61	21.22	20.55	26.74	24.78	21.59
ASWM [29]	29.59	28.36	26.32	29.12	27.23	25.27	24.01	22.56	21.22	26.54	25.15	23.19
SDOOD [30]	30.02	28.54	26.66	29.55	27.14	25.64	23.73	22.18	21.01	26.41	24.25	22.78
SBF [31]	30.04	27.18	23.41	29.17	27.03	24.02	23.04	21.99	20.49	25.91	24.66	22.84
CEF [32]	30.11	28.22	26.75	29.22	27.32	25.83	23.92	22.69	21.22	26.16	24.16	22.93
AEPWM [33]	30.77	29.01	28.03	29.75	28.11	26.62	24.05	23.08	21.75	27.65	26.61	24.78
Proposed	**30.81**	**29.95**	**28.54**	**30.01**	**28.66**	**27.48**	**24.22**	**23.63**	**22.36**	**27.84**	**26.4**	**24.82**

Regarding the SSIM metric, the comparative results presented in tabular form in Table 4 and visualized graphically in Figure 7 demonstrate that the filter method proposed significantly outperforms alternative filtering algorithms. This finding suggests the proposed approach exhibits superior capability in preserving edge structures and other fine-grained details within the imagery data.

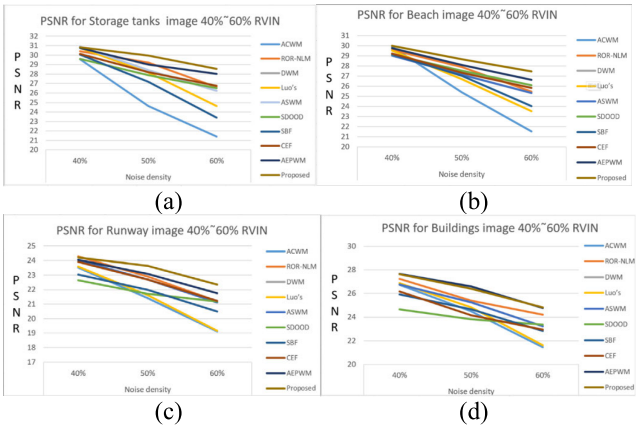

FIGURE 6. (a) PSNR for Storage tanks image 40%˜60% RVIN, (b) PSNR for Beach image 40%˜60% RVIN, (c) PSNR for Runway image 40%˜60% RVIN, (d) PSNR for Buildings image 40%˜60% RVIN.

TABLE 4. SSIM value for different images corrupted when RVIN 40%˜60%.

Method	playground			Runway			Airplane2			Intersection		
	40%	50%	60%	40%	50%	60%	40%	50%	60%	40%	50%	60%
ACWM [6]	0.877	0.765	0.584	0.812	0.707	0.548	0.737	0.647	0.498	0.809	0.706	0.569
DWM [12]	0.915	0.877	0.811	0.823	0.776	0.721	0.684	0.632	0.569	0.812	0.723	0.643
ROR-NLM [22]	0.906	0.812	0.811	0.856	0.821	0.744	0.739	0.662	0.586	0.801	0.743	0.691
Luo's [28]	0.812	0.881	0.758	0.825	0.749	0.718	0.665	0.544	0.498	0.735	0.701	0.636
ASWM [29]	0.922	0.872	0.779	0.803	0.761	0.707	0.715	0.633	0.534	0.806	0.726	0.654
SDOOD [30]	0.882	0.841	0.742	0.843	0.764	0.719	0.656	0.545	0.488	0.729	0.674	0.628
SBF [31]	0.911	0.861	0.805	0.905	0.854	0.822	0.797	0.695	0.641	0.827	0.754	0.718
CEF [32]	0.916	0.885	0.763	0.855	0.813	0.731	0.716	0.642	0.562	0.823	0.766	0.685
AEPWM [33]	0.881	0.746	0.682	0.89	0.856	0.815	0.753	0.706	0.601	0.809	0.768	0.699
Proposed	**0.934**	**0.909**	**0.877**	**0.935**	**0.922**	**0.880**	**0.814**	**0.778**	**0.719**	**0.877**	**0.811**	**0.739**

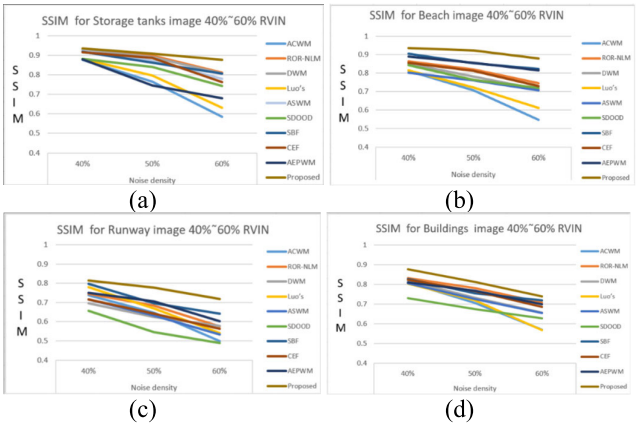

FIGURE 7. (a) SSIM for Storage tanks image 40%˜60% RVIN, (b) SSIM for Beach image 40%˜60% RVIN, (c) SSIM for Runway image 40%˜60% RVIN, (d) SSIM for Buildings image 40%˜60% RVIN.

To assess the visual impact of the filter and time assessment, denoising experiments on remote sensing images of Playground were conducted, as illustrated in Fig. 8, and PSNR and SSIM values are in Table 5.

C. ABLATION EXPERIMENTS

To perform an ablation experiment and prove the importance of our proposed study we did a comparison of our hybrid denoting method with an Edge direction filter and LCI filter.

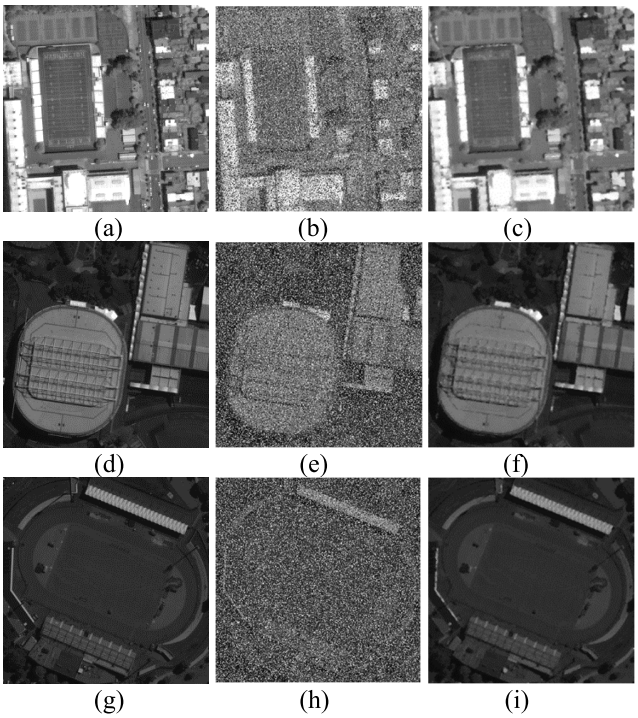

FIGURE 8. Filtering effects of proposed method on remote sensing Playground Images: (a), (d), (g) Original of Playground image, (b), (e), (h) Images with 50% RVIN, (c), (f), (i) Denoising Images.

TABLE 5. PSNR and SSIM value for Playground images corrupted when RVIN 30%˜60%.

Noise density	40%			50%			60%		
	PSNR	SSIM	T/m	PSNR	SSIM	T/m	PSNR	SSIM	T/m
Playground-1	31.34	0.940	1.21	29.83	0.902	1.29	27.73	0.792	1.36
Playground-2	22.92	0.870	1.35	22.57	0.837	1.42	21.35	0.696	1.47
Playground-3	30.17	0.904	1.27	29.01	0.882	1.33	28.01	0.776	1.38

The results of method indicate that the efficacy of denoising in method surpasses that of the old filters outlined in Table 6.

TABLE 6. Hybrid denoting method with Edge direction filter and LCI filter.

Method	Storage tanks Image		Pepper Image	
	PSNR	SSIM	PSNR	SSIM
Edge Direction filter	29.02	0.877	28.31	0.806
LCI Filter	29.59	0.911	29.12	0.885
Proposed (RVIN = LCI + EDGE)	30.81	0.934	30.01	0.935

V. CONCLUSION

The proposed method for removing random-value impulse noise (RVIN) comprises detection and removal stages. In the initial stage, the pixels of the corrupted image were categorized into multiple groups based on their distinct characteristics. An adaptive threshold recognizes the noise in each pixel group. For the noisy pixels in the flat and detailed areas, an edge-direction of median filter has been developed to recover the grayscale value of these pixels. The value of the plain point remained unchanged, and the filtering algorithm filtered the noise pixels. several simulations have demonstrated that the proposed approach is effective in

removing RVIN from natural, medical, and remote sensing images. The performance of the proposed algorithm remains stable and robust, even in the presence of elevated noise levels. The ability to denoise has improved compared to traditional filters.

In this study, the proposed method with improved LCI denoising was developed to enhance the quality of images by suppressing noise while preserving local contrast and details. However, our proposed method of denoising also has some limitations which need to be solved in the future:

- Loss of fine details: While LCI denoising can preserve some fine details, it can also lead to losing some fine details in an image. This is because LCI denoising algorithms work by averaging pixel values, which can lead to the smoothing of fine details.
- Performance dependence on image content: The effectiveness of LCI denoising depends on the image's content. LCI denoising may not be as effective in images with complex textures or patterns, or in areas of an image with low contrast.
- Computational complexity: LCI denoising algorithms can be computationally intensive, especially for large images or videos, and may require significant computing resources.
- Over-smoothing and under-smoothing: LCI denoising can result in over-smoothing or under-smoothing in some regions of an image, leading to the loss of important information or details.

Limited to denoising: LCI denoising is primarily designed to remove image noise. However, it may not be effective in enhancing other aspects of image quality, such as brightness or color saturation.

REFERENCES

[1] Q. Zhang and H. Wang, "A novel data-based stochastic distribution control for non-Gaussian stochastic systems," *IEEE Trans. Autom. Control*, vol. 67, no. 3, pp. 1506–1513, Mar. 2022.
[2] X. Yin, Q. Zhang, H. Wang, and Z. Ding, "RBFNN-based minimum entropy filtering for a class of stochastic nonlinear systems," *IEEE Trans. Autom. Control*, vol. 65, no. 1, pp. 376–381, Jan. 2020.
[3] S. Sadrizadeh, H. Otroshi-Shahreza, and F. Marvasti, "Impulsive noise removal via a blind CNN enhanced by an iterative post-processing," *Signal Process.*, vol. 192, Mar. 2022, Art. no. 108378.
[4] H. Hwang and R. A. Haddad, "Adaptive median filters: New algorithms and results," *IEEE Trans. Image Process.*, vol. 4, no. 4, pp. 499–502, Apr. 1995.
[5] T. Chen and H. Ren Wu, "Adaptive impulse detection using center-weighted median filters," *IEEE Signal Process. Lett.*, vol. 8, no. 1, pp. 1–3, Jan. 2001.
[6] T.-C. Lin, "A new adaptive center weighted median filter for suppressing impulsive noise in images," *Inf. Sci.*, vol. 177, no. 4, pp. 1073–1087, Feb. 2007.
[7] S. Sadrizadeh, N. Zarmehi, E. A. Kangarshahi, H. Abin, and F. Marvasti, "A fast iterative method for removing impulsive noise from sparse signals," *IEEE Trans. Circuits Syst. Video Technol.*, vol. 31, no. 1, pp. 38–48, Jan. 2021.
[8] N. Singh, T. Thilagavathy, R. T. Lakshmipriya, and O. Umamaheswari, "Some studies on detection and filtering algorithms for the removal of random valued impulse noise," *IET Image Process.*, vol. 11, no. 11, pp. 953–963, Nov. 2017.
[9] R. Garnett, T. Huegerich, C. Chui, and W. He, "A universal noise removal algorithm with an impulse detector," *IEEE Trans. Image Process.*, vol. 14, no. 11, pp. 1747–1754, Nov. 2005.
[10] M. Huang, J. Zou, Y. Zhang, U. A. Bhatti, and J. Chen, "Efficient click-based interactive segmentation for medical image with improved plain-ViT," *IEEE J. Biomed. Health Informat.*, vol. 1, no. 1, pp. 1–12, Jun. 2024.
[11] U. A. Bhatti, S. Marjan, A. Wahid, M. S. Syam, M. Huang, H. Tang, and A. Hasnain, "The effects of socioeconomic factors on particulate matter concentration in China's: New evidence from spatial econometric model," *J. Cleaner Prod.*, vol. 417, Sep. 2023, Art. no. 137969.
[12] Y. Dong and S. Xu, "A new directional weighted median filter for removal of random-valued impulse noise," *IEEE Signal Process. Lett.*, vol. 14, no. 3, pp. 193–196, Mar. 2007.
[13] Q. Chen, M. Huang, H. Wang, and G. Xu, "A feature discretization method based on fuzzy rough sets for high-resolution remote sensing big data under linear spectral model," *IEEE Trans. Fuzzy Syst.*, vol. 30, no. 5, pp. 1328–1342, May 2022.
[14] J. R. Chang, Y. Chen, C. Lo, and H. Chen, "An advanced AFWMF model for identifying high random-V valued impulse noise for image processing," *Appl. Sci.*, vol. 11, no. 15, pp. 7021–7037, 2021.
[15] X. Xiao, N. N. Xiong, J. Lai, C.-D. Wang, Z. Sun, and J. Yan, "A local consensus index scheme for random-valued impulse noise detection systems," *IEEE Trans. Syst. Man, Cybern. Syst.*, vol. 51, no. 6, pp. 3412–3428, Jun. 2021.
[16] N. Singh and U. Oorkavalan, "Triple threshold statistical detection filter for removing high density random-valued impulse noise in images," *EURASIP J. Image Video Process.*, vol. 2018, no. 1, pp. 1–16, Dec. 2018.
[17] M. Nadeem, A. Hussain, A. Munir, M. Habib, and M. T. Naseem, "Removal of random valued impulse noise from grayscale images using quadrant based spatially adaptive fuzzy filter," *Signal Process.*, vol. 169, Apr. 2020, Art. no. 107403.
[18] Y. Chen, Y. Zhang, H. Shu, J. Yang, L. Luo, J.-L. Coatrieux, and Q. Feng, "Structure-adaptive fuzzy estimation for random-valued impulse noise suppression," *IEEE Trans. Circuits Syst. Video Technol.*, vol. 28, no. 2, pp. 414–427, Feb. 2018.
[19] L. Afraites, A. Hadri, A. Laghrib, and M. Nachaoui, "A weighted parameter identification PDE-constrained optimization for inverse image denoising problem," *Vis. Comput.*, vol. 38, no. 8, pp. 2883–2898, Aug. 2022.
[20] S. Rawat, K. P. S. Rana, and V. Kumar, "A novel complex-valued convolutional neural network for medical image denoising," *Biomed. Signal Process. Control*, vol. 69, Aug. 2021, Art. no. 102859.
[21] P. J. S. Sohi, N. Sharma, B. Garg, and K. V. Arya, "Noise density range sensitive mean-median filter for impulse noise removal," in *Advances in Intelligent Systems and Computing*. Cham, Switzerland: Springer, 2021, pp. 150–162.
[22] R. Kosarevych, O. Lutsyk, and B. Rusyn, "Detection of pixels corrupted by impulse noise using random point patterns," *Vis. Comput.*, vol. 38, no. 11, pp. 3719–3730, Nov. 2022.
[23] T. Yamaguchi, A. Suzuki, and M. Ikehara, "Detail preserving mixed noise removal by DWM filter and BM3D," *IEICE Trans. Fundamentals Electron., Commun. Comput. Sci.*, vol. 11, no. 11, pp. 2451–2457, 2017.
[24] W. Dong, P. Wang, W. Yin, G. Shi, F. Wu, and X. Lu, "Denoising prior driven deep neural network for image restoration," *IEEE Trans. Pattern Anal. Mach. Intell.*, vol. 41, no. 10, pp. 2305–2318, Oct. 2019.
[25] J. Revaud, P. Weinzaepfel, Z. Harchaoui, and C. Schmid, "EpicFlow: Edge-preserving interpolation of correspondences for optical flow," in *Proc. IEEE Conf. Comput. Vis. Pattern Recognit. (CVPR)*, Jun. 2015, pp. 1164–1172.
[26] K. A. AlAfandy, H. Omara, M. Lazaar, and M. A. Achhab, *Machine Learning-Computational Intelligence and Applications for Pandemics and Healthcare*. Hershey, PA, USA: IGI Global, 2022, pp. 83–113.
[27] Q. Chen, M. Huang, and H. Wang, "A feature discretization method for classification of high-resolution remote sensing images in coastal areas," *IEEE Trans. Geosci. Remote Sens.*, vol. 59, no. 10, pp. 8584–8598, Oct. 2021.
[28] W. Luo, "A new efficient impulse detection algorithm for the removal of impulse noise," *IEICE Trans. Fundamentals Electron., Commun. Comput. Sci.*, vol. 88, no. 10, pp. 2579–2586, Oct. 2005.
[29] S. Akkoul, R. Ledee, R. Leconge, and R. Harba, "A new adaptive switching median filter," *IEEE Signal Process. Lett.*, vol. 17, no. 6, pp. 587–590, Jun. 2010.
[30] A. S. Awad, "Standard deviation for obtaining the optimal direction in the removal of impulse noise," *IEEE Signal Process. Lett.*, vol. 18, no. 7, pp. 407–410, Jul. 2011.

[31] C.-H. Lin, J.-S. Tsai, and C.-T. Chiu, "Switching bilateral filter with a texture/noise detector for universal noise removal," *IEEE Trans. Image Process.*, vol. 19, no. 9, pp. 2307–2320, Sep. 2010.
[32] U. Ghanekar, A. K. Singh, and R. Pandey, "A contrast enhancement-based filter for removal of random valued impulse noise," *IEEE Signal Process. Lett.*, vol. 17, no. 1, pp. 47–50, Jan. 2010.
[33] N. Iqbal, S. Ali, I. Khan, and B. M. Lee, "Adaptive edge preserving weighted mean filter for removing random-valued impulse noise," *Symmetry*, vol. 11, no. 3, p. 395, Mar. 2019.

EMADALDEN ALHATAMI received the M.S. degree in computer science from Hefei University, Hefei, Anhui, China, in 2020. He is currently pursuing the Ph.D. degree in information and communication engineering with Hainan University, Haikou, China.

BHATTI UZAIR ASLAM (Senior Member, IEEE) was born in 1986. He received the Ph.D. degree in information and communication engineering from Hainan University, Haikou, Hainan, China, in 2019. He finished his postdoctoral research at Nanjing Normal University, in implementing Clifford algebra algorithms in analyzing the geo spatial data using AI. He is currently an Associate Professor with Hainan University. His research interests include pattern recognition, image processing, and machine learning. He has published more than 80 research articles in these fields.

MENGXING HUANG (Member, IEEE) received the Ph.D. degree in system engineering from Northwestern Polytechnical University, Xi'an, China, in 2007.

He then joined the Research Institute of Information Technology, Tsinghua University, as a Postdoctoral Researcher. In 2009, he joined Hainan University, Haikou, China, where he is currently a Professor, the Ph.D. Supervisor, and the Dean of the School of Information and Communication Engineering. He is also the Director of marine information field with the State Key Laboratory of Marine Resource Utilization in South China Sea and the Team Leader of the information awareness fusion and intelligent service in Hainan. He has authored and co-authored more than 180 academic articles as the first or corresponding author. He has reported 36 licensed invention patents, 96 software copyrights, and published three monographs and one translation. His research interests include big data and intelligent information processing, multisource information awareness and fusion, artificial intelligence, and smart services. He was a recipient of the first prize and second prize of Hainan Science and Technology Progress.

SILING FENG received the Ph.D. degree in computer software and theory from the University of Electronic Science and Technology of China, Chengdu, China, in 2014. She is currently a Professor and the Ph.D. Supervisor of the School of Information and Communication Engineering, Hainan University, Haikou, China. Her research interests include intelligent computing, big data analysis, and intelligent recommendation.